Metallic Microswimmers Driven up the Wall by Gravity

Quentin Brosseau[1], Florencio Balboa Usabiaga[2], Enkeleida Lushi[3], Yang Wu[4], Leif Ristroph[1], Michael D. Ward[4], Michael J. Shelley[1,2] and Jun Zhang[1,5,6]

[1] *Applied Mathematics Laboratory, Courant Institute, New York University, NY NY 10012, USA,*
[2] *Flatiron Institute, Simons Foundation, NY NY 10010, USA*
[3] *Dept. of Math. Sciences, New Jersey Institute of Technology, Newark NJ 07102, USA*
[4] *Dept. of Chemistry, New York University, NY NY 10012, USA*
[5] *Dept. of Physics, New York University, NY NY 10003, USA*
[6] *NYU-ECNU Institute of Physics, New York University Shanghai, Shanghai 200062, China*

(Dated: April 3, 2021)

I. EXPERIMENTAL DETAILS (SAMPLE PREPARATION)

The nanorods are synthesized by a templating method on Anodic Aluminium Oxide (AAO) membranes (Whatman Anodisc™ 47) with a typical pore diameter of $0.3\,\mu$m. Prior to the electrodeposition, one side of the AAO membrane is sealed by thermo-evaporation of a 150 nm thick layer of silver (BAL-TEC MCS 010 Multi Control System).

The electrodeposition is made in three steps using a three-electrodes method:

- A layer of silver is deposited at -1 V from an aqueous solution of silver cyanide (0.0186 M, AgCN, Thermo Fisher Scientific Inc.), potassium cyanide (0.1233 M, KCN, Thermo Fisher Scientific Inc.) and potassium pyrophosphate (0.0304 M, $K_4P_2O_7$, Sigma-Aldrich, Co. LLC) to prevent leakages.
- A layer of gold is deposited at -0.92V from a commercial plating solution (OROTEMP 24 RTU Rack from TECHNIC INC).
- In the case of Au-Rh symmetric nanorods, a layer of rhodium is deposited at -0.4 V from a commercial plating solution (Techni Rhodium RTU from TECHNIC INC). In this case, the deposition charges of gold C_{Au} and Rhodium C_{Rh} are 16 C and 68 C, respectively.

  In the case of Au-Pt nanorods, a layer of platinum is deposited at -0.4 V from an aqueous solution of ammonium hexachloroplatinate (IV) (0.010 M, $(NH_3)_2PtCl_6$, Alfa Aesar) and sodium phosphate dibasic dihydrate (0.020 M,Na_2HPO_4, Sigma-Aldrich, Co. LLC). The deposition charges of gold and platinum are $C_{\mathrm{Au}} = 7.2$ C and platinum $C_{\mathrm{Pt}} = 26$ C for symmetric rods and $C_{\mathrm{Au}} = 24$ C and $C_{\mathrm{Pt}} = 9$ C for long gold segment rods.

The silver layer is etched away in a solution of HNO_3 (1 M), and the membrane is dissolved in a NaOH solution (5 M). The resulting suspension with nanorods is purified through a repeated centrifugation/dilution process.

A. Rods' parameters

Table I shows the geometry of the rods, their diffusion coefficients (D_t and D_r) and their swimming speeds (V_0) at different H_2O_2 concentration.

TABLE I: Table of geometrical and physical properties of symmetric Au-Rh nanorods and the two Au-Pt nanorod types with gold and platinum fractions ($l_{\mathrm{Au}} : l_{\mathrm{Pt}}$).

Batch	D_t [μm^2/s]	D_r [1/s]	V_0 [μm/s]	H_2O_2%
Au-Rh(1:1) $L = 2.5\,\mu$m	0.3	1.04	0	0
Au-Rh(1:1) $L = 2.5\,\mu$m	0.3	1.04	2.7 ± 0.3	10
Au-Rh(1:1) $L = 2.5\,\mu$m	0.3	1.04	4.5 ± 0.5	15
Au-Rh(1:1) $L = 2.5\,\mu$m	0.3	1.04	8.0 ± 1.0	30
Au-Pt(1:1) $L = 2\,\mu$m	0.25	0.6	6.1 ± 0.8	15
Au-Pt(3:1) $L = 2\,\mu$m	0.25	0.6	6.5 ± 0.7	20

II. CENTER OF HYDRODYNAMIC STRESS (COH)

The choice of a tracking point to describe the orientation of a body cannot affect the dynamics of the system (of course!) but it affects the structure of the equations of motion. In systems with inertia, it is natural to choose the center of mass (CoM) as the tracking point because the translational and rotational contributions to the kinetic energy decouple. For particles immersed in a Stokes flow, where inertia does not play a role, other choices are more convenient. This issue was explored by Brenner in the 1960s [1] and later expanded and clarified by García Bernal and García de la Torre [2]. We reproduce here their principal results for completeness.

Consider a rigid body immersed in a three dimensional Stokes flow. Its dynamics can be described by the linear and angular velocity about a tracking point 1. The linear system that relates the force and torque ($\boldsymbol{F}_1$ and $\boldsymbol{\tau}_1$) with the linear and angular velocities ($\boldsymbol{V}_1$ and $\boldsymbol{\omega}_1$) is

$$\begin{pmatrix} \boldsymbol{V}_1 \\ \boldsymbol{\omega}_1 \end{pmatrix} = \begin{pmatrix} \boldsymbol{M}_{VF,1} & \boldsymbol{M}_{\omega F,1}^T \\ \boldsymbol{M}_{\omega F,1} & \boldsymbol{M}_{\omega\tau,1} \end{pmatrix} \begin{pmatrix} \boldsymbol{F}_1 \\ \boldsymbol{\tau}_1 \end{pmatrix}, \tag{1}$$

where the 3×3 mobility components $\boldsymbol{M}_{VF,1}$ etc. depend on the tracking point chosen to describe the motion as indicated by the subindex 1. The force, torque and velocities defined at a second tracking point are

$$\boldsymbol{F}_2 = \boldsymbol{F}_1, \quad \boldsymbol{\tau}_2 = \boldsymbol{\tau}_1 - \boldsymbol{r} \times \boldsymbol{F}_1, \tag{2}$$

$$\boldsymbol{V}_2 = \boldsymbol{V}_1 + \boldsymbol{\omega}_1 \times \boldsymbol{r}, \quad \boldsymbol{\omega}_2 = \boldsymbol{\omega}_1, \tag{3}$$

where $\boldsymbol{r}$ is the vector that goes from the first to the second tracking point, see Fig. 1 left. We can use (1)-(3) to show that the mobility components transform between tracking points like [2]

$$\boldsymbol{M}_{\omega\tau,2} = \boldsymbol{M}_{\omega\tau,1}, \tag{4}$$

$$\boldsymbol{M}_{\omega F,2} = \boldsymbol{M}_{\omega F,1} + \boldsymbol{M}_{\omega\tau,1} \times \boldsymbol{r} \tag{5}$$

$$\boldsymbol{M}_{VF,2} = \boldsymbol{M}_{VF,1} - \boldsymbol{r} \times (\boldsymbol{M}_{\omega\tau,1} \times \boldsymbol{r}) + \boldsymbol{M}_{\omega F,1}^T \times \boldsymbol{r} - \boldsymbol{r} \times \boldsymbol{M}_{\omega F,1}, \tag{6}$$

where the cross product between a 3×3 matrix and a vector is defined, using the Levi-Civita symbol, as $(\boldsymbol{M} \times \boldsymbol{r})_{ij} = M_{ik}\epsilon_{jkl}r_l$ and $\boldsymbol{r} \times \boldsymbol{M} = -\boldsymbol{M} \times \boldsymbol{r}$.

For any body shape there is a special tracking point where the coupling matrix $\boldsymbol{M}_{\omega F}$ is symmetric. This point is called in the literature the *Center of Mobility* [2]. The location of the center of mobility with respect to an arbitrary tracking point can be found by solving for $i \neq j$ the linear system [3]

$$\left(\epsilon_{ikl} \left(\boldsymbol{M}_{\omega\tau}\right)_{jk} - \epsilon_{jkl} \left(\boldsymbol{M}_{\omega\tau}\right)_{ik}\right) r_l = \left(\boldsymbol{M}_{\omega F}\right)_{ij} - \left(\boldsymbol{M}_{\omega F}\right)_{ji}, \tag{7}$$

where the mobility components are calculated at the original tracking point. For bodies of enough symmetry (e.g. axisymmetric bodies), the coupling matrix $\boldsymbol{M}_{\omega F}$ vanishes at the center of mobility. In such cases, the center of mobility is also called the *Center of Hydrodynamic stress* (CoH). Therefore the CoH can be found from (7) if it exists.

For two dimensional systems (or three dimensional particles constrained to move in the xy plane), the CoH always exists and it corresponds to the point where a torque applied out of the plane does not generate translations. We can compute its location respect an arbitrary tracking point with [3]

$$\boldsymbol{r} = \left(\frac{M_{\omega_z F_y}}{M_{\omega_z \tau_z}}, \frac{M_{\omega_z F_x}}{M_{\omega_z \tau_z}}\right). \tag{8}$$

As discussed in the main text, we use this tracking point to uncouple the rotational equation of motion from translations.

The figure 1 right shows that if the hydrodynamic interactions with the wall are neglected the density mismatch is not enough to explain the orientation bias of the rods observed in the experiments.

III. EFFECT OF THE SWIMMING SPEED

In this section we estimate the critical swimming speed that allows upward movement (i.e. $\langle V_x \rangle > 0$). When the reorienting torque is very large (i.e. $K \gg 1$) the rods are aligned with the x-axis and the critical swimming speed coincides with the speed of sedimentation along the wall $V_{0c} = \mu_\parallel mg \sin\beta$, here $\mu_\parallel$ is the tangential mobility of the

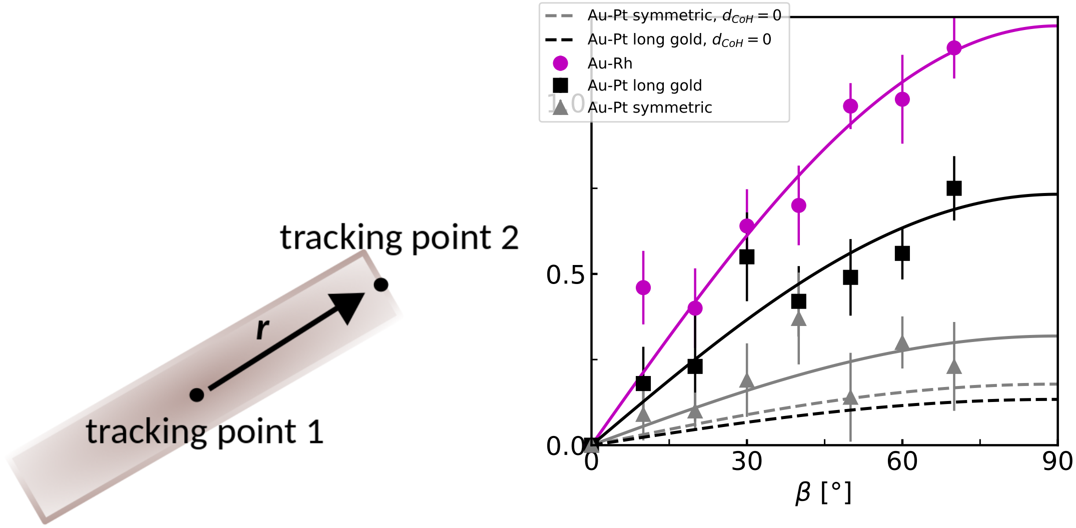

FIG. 1: **(Left)** Sketch of a rigid body with two tracking points. **(Right)** Reproduction of the figure 6c from the main text, K vs. β, for experiments (symbols) and theoretical fits (continuum lines). We include the theoretical prediction assuming $d_{\mathrm{CoH}} = 0$ (dashed lines) which reveals the important effect of a finite d_{CoH} to fit the experimental results.

rod. For weak reorienting torques, $K \lessapprox 1$, like in our experiments the critical swimming speed will be larger as the rods are not always aligned with the x-axis. We use our mechanical model to estimate V_{0c} in this regime. The linear velocity of the Center of Hydrodynamic stress (CoH) is (from eq. [1] in the main text)

$$\boldsymbol{V} = \begin{pmatrix} V_0 \cos\theta \\ V_0 \sin\theta \end{pmatrix} + \boldsymbol{M}_{VF}\boldsymbol{F} + [\text{noise terms}], \tag{9}$$

note that the torque does not appear explicitly because we use the CoH as the tracking point. The mobility depends on the angle θ between the rod and the x-axis

$$\boldsymbol{M}_{VF} = \begin{pmatrix} \cos\theta & -\sin\theta \\ \sin\theta & \cos\theta \end{pmatrix} \begin{pmatrix} \mu_\parallel & 0 \\ 0 & \mu_\perp \end{pmatrix} \begin{pmatrix} \cos\theta & -\sin\theta \\ \sin\theta & \cos\theta \end{pmatrix}^T, \tag{10}$$

where $\mu_\parallel$ and $\mu_\perp$ are the parallel and perpendicular mobilities (for a slender body $\mu_\parallel = 2\mu_\perp$). Therefore, the velocity along the x-axis is

$$V_x = V_0 \cos\theta + \mu_\perp F_x + (\mu_\parallel - \mu_\perp) F_x \cos^2\theta + [\text{noise terms}], \tag{11}$$

and after integrating over orientations we get

$$\langle V_x \rangle = \frac{1}{2\pi}\int_{-\pi}^{\pi} V_x P(\theta)\mathrm{d}\theta = V_0 \frac{I_1(K)}{I_0(K)} + \frac{1}{2}\left[(\mu_\parallel + \mu_\perp) + (\mu_\parallel - \mu_\perp)\frac{I_2(K)}{I_0(K)}\right] F_x, \tag{12}$$

where $I_n(x)$ are modified Bessel functions of the first kind and we used the angle distribution, $P(\theta) = \exp(K\cos\theta)/(2\pi I_0(K))$, obtained from the eq. [2] in the main text. To first order in K

$$\langle V_x \rangle = \frac{V_0 K}{2} + \frac{\mu_\parallel + \mu_\perp}{2} F_x. \tag{13}$$

Upward swimming ($\langle V_x \rangle > 0$) is possible when $K > -(\mu_\parallel + \mu_\perp)F_x/V_0$, i.e. when K is larger than the ratio between the sedimentation velocity and the intrinsic swimming speed. After substituting the values of the gravitational force, $F_x = -mg\sin\beta$, and $K = r_0 mg \sin\beta\cos\alpha/k_B T$, we obtain the critical swimming speed for weak reorienting torques

$$V_{0c} = \frac{(\mu_\parallel + \mu_\perp)k_B T}{r_0 \cos\alpha}. \tag{14}$$

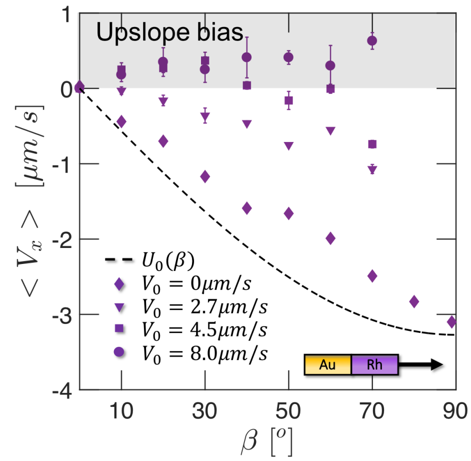

FIG. 2: Experimental results (symbols) of gravitaxis of bottom-heavy rods for several swimming speeds controlled with the H_2O_2 concentration. The dashed line represents the sedimentation velocity estimation $U_0(\beta) = -\mu_\parallel mg \sin\beta$.

Interestingly, in this regime the critical swimming speed is independent of the particle mass and the inclination of the wall, as long as $mg\sin\beta > 0$, because the gravitational pulling force contributes both to reorient the particle upwards and to pull it downwards. The length of the lever arm, r_0, is critical.

Using the mobility approximation of a cylinder in bulk ($\mu_\parallel = (\log(L/r) - 0.72)/(2\pi\eta L)$ and $\mu_\perp = \mu_\parallel/2$ [1]) we estimate a critical swimming speed of around $4\,\mu$m/s for our Au-Rh particles. Indeed, Fig. 2 shows that slow rods fall for all wall inclinations. Faster rods with $V_0 = 4.5\,\mu$m/s show upslope motion (shaded area) for moderate values of β. For higher swimming speeds, upslope motion is visible for all inclinations.

IV. ADDITIONAL NUMERICAL RESULTS

We provide here some additional results obtained from numerical simulations to support our claims. First, we show the tilt angle α of rods towards the wall in the left panel of figure 3. Rods with long gold segments tilt more. This is consistent with our previous investigation about the dynamic of phoretic swimmers in shear flows [4]. Note that the tilt angle is controlled by the location of the active slip along the rod and that the density difference between Au-Rh and Au-Pt plays a minimal role. We show the computed distance between the CoH and the rod's center in Fig. 3 right. The physical interpretation of these results is that the higher drag near the front of the rod displaces the center of rotation forward. Note that in the limit where a rod is pinned to the wall the anchor point will act as the center of rotation.

In simulations with Brownian noise we are able to measure the average velocity along the wall $\langle V_x \rangle$ and the orientation bias measured by K just like in the experiments. Brownian motion can be included into our model by adding a stochastic contribution, $\boldsymbol{u}_i^{\text{stoch}} = \sqrt{2k_BT/\Delta t}\left(\boldsymbol{M}^{1/2}\boldsymbol{W}\right)_i$, to the right hand side of the slip condition, Eq. 1 in the main text, and using an stochastic integrator to update the rod position and orientation [3, 5].

In the top panels of Fig. 4, we show the average velocity along the x-axis versus the wall inclination for Au-Pt and Au-Rh rods. In the bottom panels of Fig. 4, we show K versus the wall inclination β. The Au-Rh rods swim upwards for all inclinations and all swimmer types. Meanwhile, Au-Pt rods with short-gold segement and symmetric swimmers fall although their orientations show that they point upwards most of the time. Au-Pt rods with long-gold segment show a weak upward swimming bias. All these results agree qualitatively with the experiments although the numerical swimmers are better gravitactors. We note that in the simulations we model the active slip instead of solving the complicated electrochemical problem that ultimately creates the active flows. Moreover, we ignore if there are electrostatic forces between the rods and the wall which could affect the results. For these reasons we do not expect a perfect agreement between the simulations and the experimental results. The great contribution from the simulations is to show, in a perfect controlled system, the same general behavior as in the experiments.

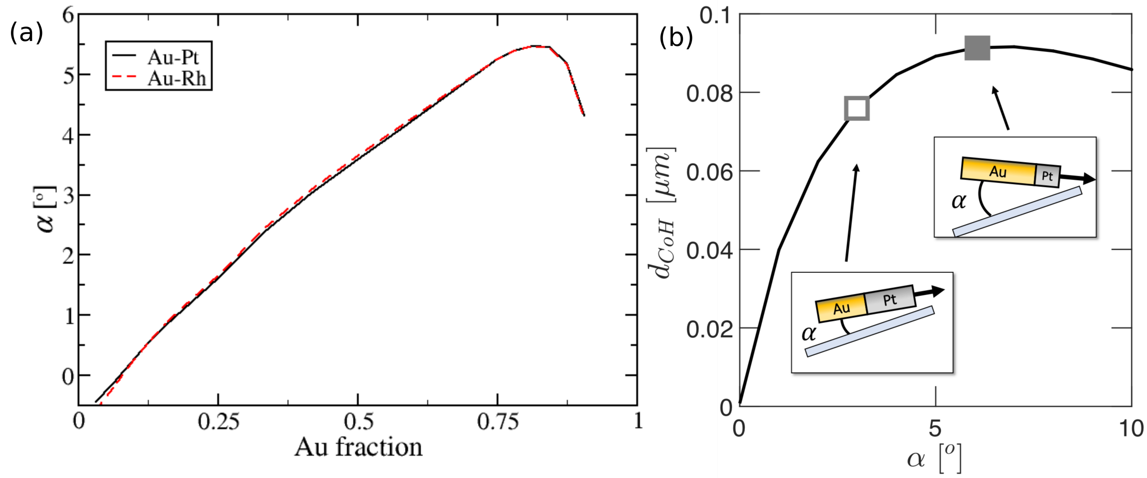

FIG. 3: Results from deterministic simulations for $L = 2\,\mu$m long rods. **(a)** tilt angle α with the wall for rods with different gold fractions. **(b)** Distance between the CoH and the rod's geometric center assuming that the rod's head is at a height $h = 0.2\,\mu$m from the wall.

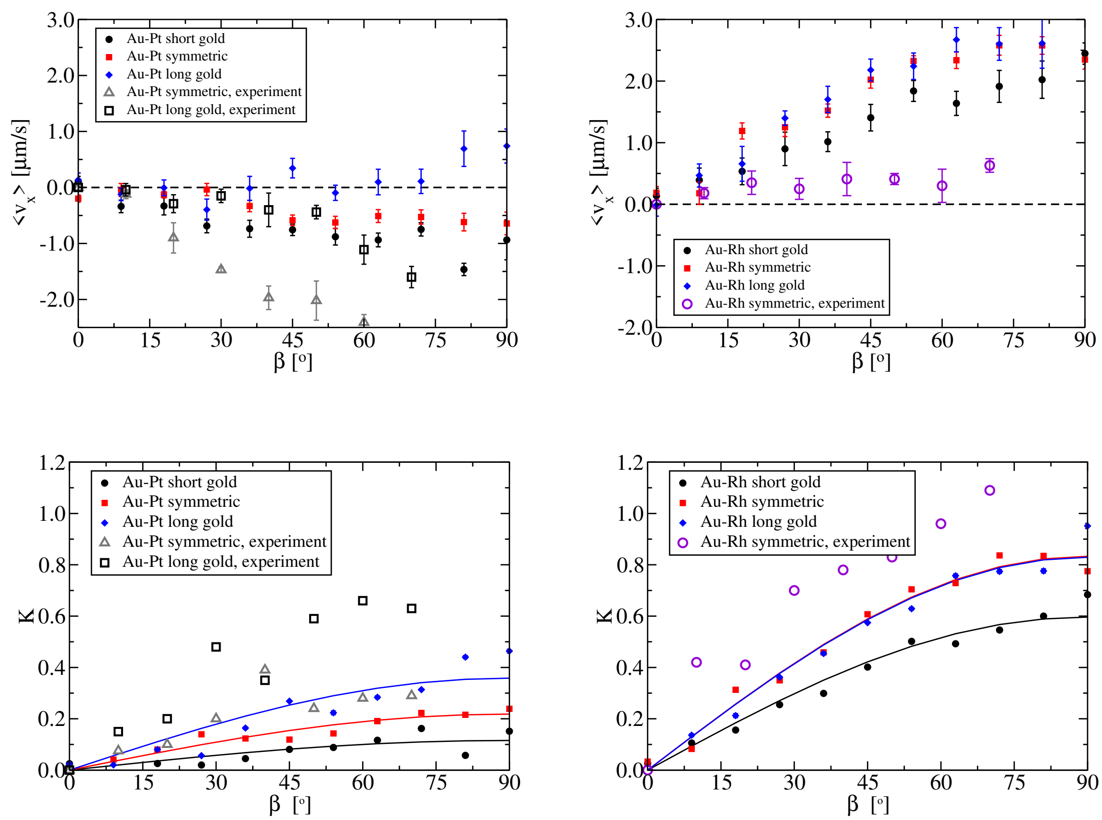

FIG. 4: Comparison between experimental results (open symbols) and Brownian simulations (full symbols) of $2\,\mu$m long rods swimming near a wall. **Top panels:** mean upward velocity versus wall inclination for Au-Pt (Left) and Au-Rh rods (Right). **Bottom panels:** K parameter versus wall inclination for Au-Pt (Left) and Au-Rh rods (Right). The continuum lines are fit of the numerical results to the theoretical formula.

[1] J. Happel and H. Brenner, *Low Reynolds number hydrodynamics* (Springer Netherlands, 1983).
[2] J. M. G. Bernal and J. G. De La Torre, Biopolymers **19**, 751 (1980).
[3] S. Delong, F. Balboa Usabiaga, and A. Donev, J. Chem. Phys. **143**, 144107 (2015).
[4] Q. Brosseau, F. Balboa Usabiaga, E. Lushi, Y. Wu, L. Ristroph, J. Zhang, M. Ward, and M. J. Shelley, Phys. Rev. Lett. **123**, 178004 (2019).
[5] B. Sprinkle, F. Balboa Usabiaga, N. A. Patankar, and A. Donev, J. Chem. Phys. **147**, 244103 (2017).